

PORE SCALE MODELING OF BRINE DEPENDENT PERMEABILITY

Janne Pedersen¹, Espen Jettestuen¹, Jan Ludvig Vinningland¹, Merete V. Madland² and Aksel Hiorth^{1,2}

¹International Research Institute of Stavanger (IRIS), ²University of Stavanger (UiS)

This paper was prepared for presentation at the International Symposium of the Society of Core Analysts held in Napa Valley, California, USA, 16-19 September, 2013

ABSTRACT

The numerical study of pore surface evolution due to precipitation and dissolution of minerals requires a reliable representation of the time dependent evolution of the pore surface, as the evolution of the pore volume and surface area impacts both permeability and effective rate equations used in the “macroscopic” modeling of porous media. In this paper we present three different implementations of a moving boundary routine and discuss them in terms of 1) conservation of mass, 2) convergence for increasing grid resolution and 3) rotational invariance. We also study growth as a function of Peclét-Damköhler number, we use the Carman-Kozeny equation to relate the predicted porosity and surface area evolution to permeability evolution. We observe that for high Peclét-Damköhler numbers the permeability reduction is more affected by a large increase in surface area than porosity loss.

INTRODUCTION

In several rock mechanical compression tests it has been observed that the permeability of the core decreases during the experiment. Part of this permeability loss is simply due to porosity loss caused by pure mechanical deformation, and part is due to chemical precipitation and dissolution processes in the pore space and/or intergranular contacts. Dissolution and precipitation will change the porosity and/or the specific surface area, which in turn affect the permeability of the rock. Flooding with seawater at 130°C through chalk cores makes the permeability drop to zero over a period of two weeks, while flooding with NaCl brine has a much lower effect on the permeability [1]. In order to predict the permeability-porosity evolution during core floods from pore scale simulations, it is necessary to have numerical methods that can describe the dynamic

evolution of the pore space as a consequence of rock-fluid interactions. The BGK lattice Boltzmann method (LBM) [2,3] is well suited to describe multiphase, reactive flow on the pore scale, and has been used in numerous studies. Lattice Boltzmann methods with a dynamic evolution of the pore space caused by reactive flows have been published [4,5], but these methods do not respect rotational invariance. By rotational invariance we mean that the growth of minerals should be independent of the orientation of the grid. In this paper we develop rotationally invariant numerical methods that allow reliable studies of changes in surface topology due to chemical reactions on the pore scale. On the pore scale diffusion is usually much faster than advection, thus it is a reasonable approximation to only consider diffusion. In this paper we study to which degree three different moving boundary routines (MBRs) fulfill conservation of mass, convergence for increased grid resolution, and rotational invariance for different Peclet-Damköhler (PeDa) numbers for the growth of an initial mineral seed in a diffusion field. We also study how porosity and surface area evolves with time, and the permeability evolution through a Carman-Kozeny relation.

METHOD

The MBRs discussed in this paper are based on the Volume of Fluid (VOF) approach where each computational cell is assigned a solid fraction (sf) ranging from 0 (empty) to 1 (completely filled). In this work we consider only one solid mineral phase, which is coupled to one aqueous chemical species. However, the MBRs presented are easily extended to more complex cases. The update in sf is given by the difference in incoming and outgoing microscopic flux at the mineral surface. The microscopic fluxes are related to the macroscopic surface flux J_r and species concentration, c , by [4]:

$$g_{\bar{\alpha}} - \tilde{g}_{\alpha} = (\omega_{\alpha} + \omega_{\bar{\alpha}}) \frac{2\vec{e}_{\bar{\alpha}} \cdot \vec{n} J_R}{c_s^2}, \quad g_{\bar{\alpha}} + \tilde{g}_{\alpha} = (\omega_{\alpha} + \omega_{\bar{\alpha}}) c, \quad (1)$$

where \tilde{g}_{α} denotes the incoming distribution function and $g_{\bar{\alpha}}$ is the distribution reflected from the surface for direction α . ω_{α} and $\omega_{\bar{\alpha}}$ are the LBM weights that distinguish between direct and diagonal links ($\omega_{\alpha} = 1/9$ for direct links, $\omega_{\alpha} = 1/36$ for diagonal links and $\omega_{\alpha} = 4/9$ for the stationary state in the d2q9 model used here, where 9 discrete directions are given on a 2 dimensional square lattice [2]). $\vec{e}_{\bar{\alpha}}$ is the discrete LBM velocity pointing away from the surface, \vec{n} is the surface normal pointing away from the surface, $\vec{n} J_R$ is the chemical reaction flux for species i , and c_s is the lattice sound speed ($1/\sqrt{3}$ for d2q9). For the surface flux we have assumed linear kinetics complemented with a simplified surface tension term giving $J_R = -k(c - c^{eq}) + a\kappa$, where k is the reaction rate, c^{eq} is the equilibrium concentration at the surface, a is the strength of the surface tension, and κ is the cell curvature. Inserting this expression into Eq. (1) yields:

$$g_{\bar{\alpha}} = \frac{1 - k_{\alpha}}{1 + k_{\alpha}} \tilde{g}_{\alpha} + \frac{k_{\alpha}}{1 + k_{\alpha}} 2\omega_{\alpha} c^{eq} + \frac{6\omega_{\alpha} a \kappa}{1 + k_{\alpha}} \vec{e}_{\alpha} \cdot \vec{n}, \quad (2)$$

where $k_{\alpha} = 3k\vec{e}_{\alpha} \cdot \vec{n}$. $PeDa$ is related to the reaction rate through $PeDa = 3kL/(\tau - 0.5)$, where L is the system length. Below we describe three MBRs that use this boundary condition formulation.

In *method 1* the surface normal is not calculated from the solid fraction, but simply assumed to behave as $\vec{e}_{\alpha} \cdot \vec{n} = 1$ for all link directions, and we put $a = 0$. The change in solid fraction is given by

$$\Delta sf = V_m^{-1} \left(\sum_{links} g_{\bar{\alpha}}^i - \tilde{g}_{\alpha}^i \right), \quad (3)$$

where V_m is the molar volume of the mineral.

Method 2 differs from method 1 only by the calculation of \vec{n} used in equation (1). The surface normal is estimated with the Elvira VOF method [6], although other methods could also be used. In this VOF method the true surface is approximated by linear segments in boundary cells, i.e. cells with $0 < sf < 1$.

Method 3 uses the subgrid VOF estimation of the surface position to approximate the distance between nearby fluid nodes and the surface. This distance is then used to interpolate the distribution functions near the wall [7]. We have used the VOF height function (HF) technique described in [8] to estimate the cell curvature used in the surface tension term.

RESULTS

The mineral growth simulations start from an initial solid seed rendered at different resolutions, similar to what is used in López et.al [9]. Figure 1 shows the growth of the initial seed when rotated 0° and 45° for $PeDa = 10$ and 100 for each of the three MBR methods. The initial concentration field used in all these simulations is a stationary solution obtained with $c = 0.6$ and rate $k = 1.67/L$ on the seed surface, a fixed boundary condition $c = 1$ and rate $k = 1667/L$ on the circular outer boundary, and an initial concentration $c = 0.7$.

All three methods conserve mass since the amount of solid mass precipitated on the surface equals the amount of mass extracted from the fluid phase. Rotational invariance is examined in Figure 1. The results show that the deviation from rotational invariance increases with increasing $PeDa$. However, method 3 shows a much smaller deviation for higher $PeDa$ than the two simpler methods. In order to obtain better rotational invariance for higher $PeDa$ numbers a surface tension term is introduced which also sets a limit on

the smallest spatial scales of the growing mineral. Hence, for increasing grid resolution the mineral shapes converge. Without this term more and more details will appear as the grid resolution increases, given that PeDa is high enough. Figure 2 shows the deviation from rotational invariance (E) as a function of grid resolution (L) for PeDa 100 with surface tension strength $a = -0.01$, for time step 12.000 at resolution 120x120 (outer circle radius of 50). We observe that as the resolution increases with a factor two, the gain in rotational invariance is a factor four for the deviation.

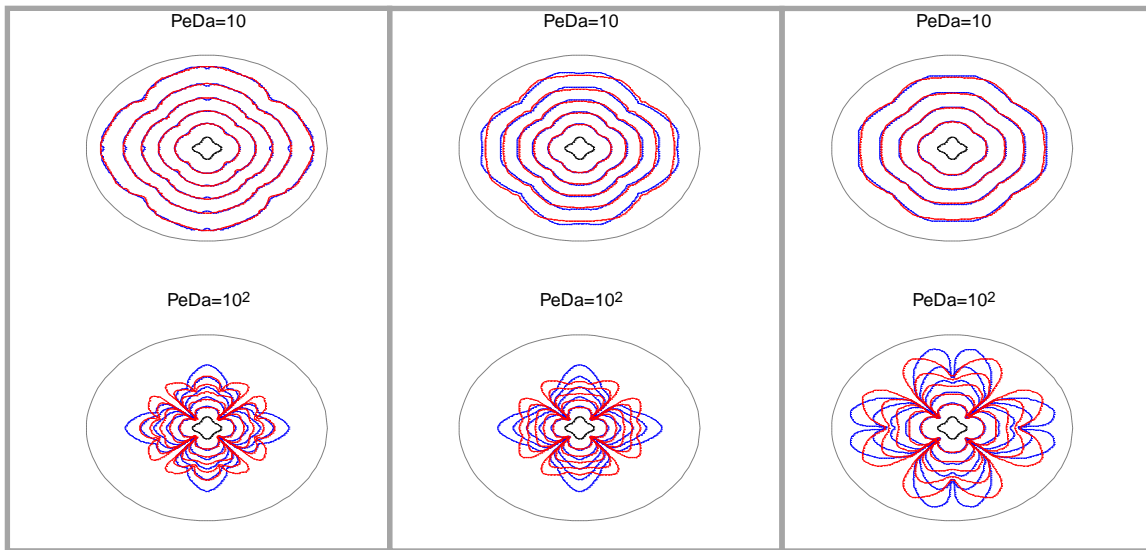


Figure 1: Rotational symmetry for PeDa 10^2 and 10 for methods 1, 2 and 3, from left to right respectively. Initial seed shown as the innermost contour.

Figure 3 shows the evolution of permeability, ε , porosity, Φ , and specific surface area (SSA), S , for different PeDa numbers for method 3 without the surface tension term (same results as shown in Figure 1.). Permeability is related to porosity and SSA through the Carman-Kozeny (CK) relation ($\varepsilon = \Phi^3 / K_0 \tau^2 S^2$). The drop in porosity and increase in surface area are faster with increasing PeDa. The SSA will increase and the permeability will decrease at an increasing rate as more details grow on the solid surface. This is shown by the changing slopes seen for PeDa = 10^4 . Edge-effects caused by approaching the outer boundary can also contribute to varying slopes at late times. Using the surface tension term would smooth the SSA evolution curves for high PeDa. For high PeDa numbers the permeability can approach zero in relatively short time.

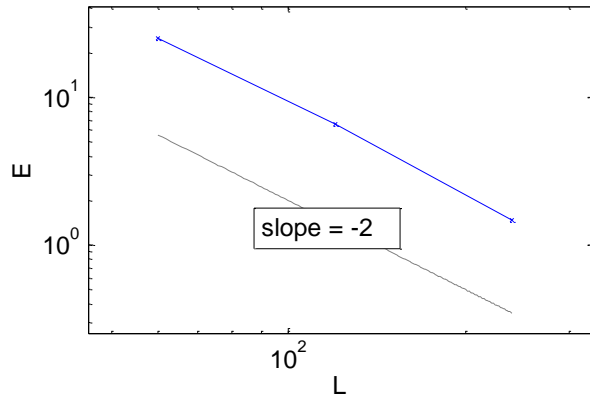


Figure 2: Deviation from rotational invariance (E) as a function of grid resolution (L). Dotted line shows a straight line with slope -2 for comparison of slopes.

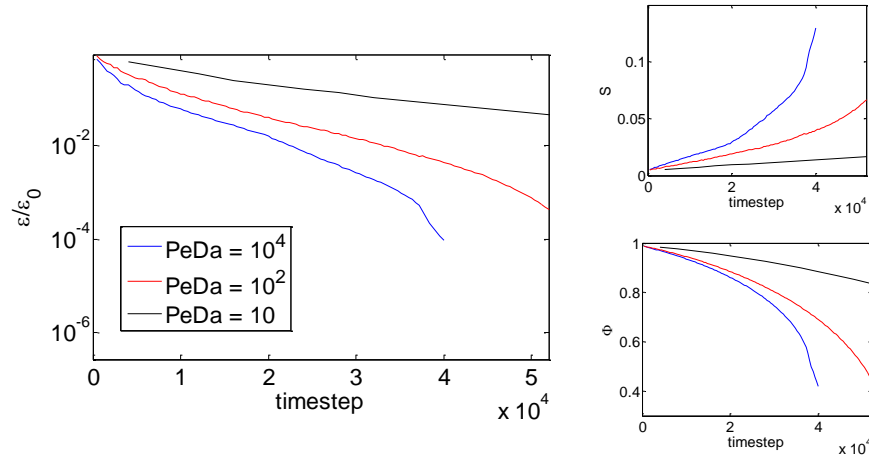


Figure 3: The evolution of the permeability based on the Carman-Kozeny relation (on the left), based on the evolution of the surface area (top right hand figure) and porosity (bottom right hand figure).

CONCLUSION

It is important to have physical consistent models that can describe how the injected water moves through the pore space, interacts with minerals, and dynamically changes the properties of the pore surface, such as changes in geometry and wettability in order to interpret lab experiments. Therefore, in this paper, we have investigated the behavior of three moving boundary routines for conservation of mass, rotational invariance, and convergence for increasing grid resolutions. All methods are mass conserving, while the subgrid VOF method (method 3) displays better rotational symmetry compared to the two simpler methods. The deviation from rotational invariance increases with increasing PeDa for all three methods. To obtain rotational invariance and convergence for high

PeDa numbers we introduce a surface tension term which sets a minimum unstable wave length that is larger than the grid resolution. For low PeDa numbers we note that methods 1 and 2 give reasonable results and might be preferred over method 3 due to computational effectivity. Method 3 shows an increasing drop in porosity (increase in SSA) for increasing PeDa numbers. The rate at which SSA increases seems to increase at the time when higher resolution details start to grow on the mineral surface for high PeDa numbers. Permeability profiles also show that the permeability can approach zero for high PeDa numbers, without a significant porosity loss.

ACKNOWLEDGEMENTS

The authors would like to thank the Research Council of Norway, BP Norge AS and the Valhall co-venturers, including Hess Norge AS, ConocoPhillips and the Ekofisk co-venturers, including Total E&P Norge AS, ENI Norge AS, Statoil Petroleum AS and Petoro AS for financial support.

REFERENCES

1. Madland, M. V., Hiorth, A., Omdal, E., Megawati, M. and Hildebrand-Habel, T. et al. Chemical Alterations Induced by Rock-Fluid Interactions When Injecting Brines in High Porosity Chalks, *Transp. Porous Med.* (2011) **87**, 679-702
2. Succi S., *The Lattice Boltzmann Equation for Fluid Dynamics and Beyond*, Oxford University Press, Oxford (2001).
3. Sukop, M. C. and Thorne D. T. *Lattice Boltzmann Modeling: An Introduction for Geoscientists and Engineers*, Springer, Netherlands (2006)
4. Verghaeghe, F., Arnout, S., Blanpain, B. and Wollants, P., Lattice-Boltzmann modeling of dissolution phenomena. *Phys. Rev. E*, (2006) **73**, 1-10.
5. Kang, Q. and Lichtner, P. C., Pore Scale Modeling of Reactive Transport Involved in Geologic CO₂ Sequestration, *Transp. Porous Med.*, (2009) **82**, 197-213
6. Pilliod Jr, J. E. and Puckett, E. G. Second-order accurate volume-of-fluid algorithms for tracking interfaces, *J. Comp. Phys.* (2004) **199**, 464-502.
7. Bouzidi, M., Firdaouss, M. and Lallemand, P., Momentum transfer of a Boltzmann-lattice fluid with boundaries, *Physics of Fluids*, (2001) **13**, 11, 3452-3459.
8. Cummins, S. J., Francois, M. and Kothe, D. B., Estimating curvature from volume fractions, *Computers and structures*, (2005) **83**, 425-434
9. López, J., Gómez, P and Hernández, J., A volume of fluid approach for crystal growth simulation, *J. Comp. Phys.* (2010) **229**, 6663-6672.